Dalton Transactions

PAPER

View Article Online
View Journal | View Issue

Check for updates

Cite this: *Dalton Trans.*, 2017, **46**, 15354

Ferritin nanocages loaded with gold ions induce oxidative stress and apoptosis in MCF-7 human breast cancer cells†

Daria Maria Monti, [a] Giarita Ferraro, [a] Ganna Petruk,[a] Laura Maiore,[b] Francesca Pane,[a] Angela Amoresano,[a] Maria Agostina Cinellu [b] and Antonello Merlino *[a]

Received 30th June 2017,
Accepted 5th October 2017

DOI: 10.1039/c7dt02370g

rsc.li/dalton

Two anticancer gold(III) compounds, **Au$_2$phen** and **Auoxo4**, were encapsulated within a ferritin nanocage. The gold-compound loaded proteins were characterized by UV-Vis spectroscopy, inductively coupled plasma mass spectrometry and circular dichroism. X-ray crystallography shows that the compounds degrade upon encapsulation and gold(I) ions bind Ft within the cage, close to the side chains of Cys126. The gold-encapsulated nanocarriers are cytotoxic to human cancer cells. Au(I)-loaded Ft, obtained upon the encapsulation of **Au$_2$phen** within the cage, induces oxidative stress activation, which finally leads to apoptosis in MCF-7 cells.

Introduction

There is currently great interest in the development of new biomaterials that can be used to selectively deliver drugs to their final targets. Nature offers a variety of protein scaffolds that self-assemble to form cages within the nanometer scale and can be used to trap drugs in their interior cavity. Among these systems, a special position is occupied by the ferritin superfamily.[1] The mammalian iron-storage protein ferritin (Ft) is a heteropolymer consisting of two genetically distinct subunits, called the H-chain (~21 kDa) and L-chain (~19 kDa). Ft is a four-helix bundle protein which forms a cage of 24 monomers (Ft nanocage), which is characterized by an octahedral 432 symmetry, with internal and external diameters of ~80 and ~120 Å, respectively.[2] Ft is fundamental for life: its role is to protect cells from oxidative damage caused by the harmful products of the Fenton reaction and to store iron.

A Ft cage is an attractive carrier for targeted drug delivery,[1,3,4] since it is not expensive, available in a large amount, easy to purify, biocompatible, stable and monodisperses in the bloodstream. Ft is also characterized by a small size compared to other potential drug carriers; its structure allows chemical modifications, including the conjugation of different chemical groups.[5] Most importantly, it is recognized and internalized by specific receptors which are over-expressed in a variety of malignant cells: the transferrin receptor 1 (TfR1) and Scara5.[6–8]

It was earlier shown that cisplatin[9] and the second generation Pt antitumor drug carboplatin[10] can be encapsulated in the cavity of apoferritin (AFt); the resulting drug-loaded proteins have well documented cytotoxic effects on tumor cells (pheochromocytoma, gastric, breast, cervix and melanoma cells),[11–14] demonstrating the efficiency of Ft as a carrier of these drugs to malignant cells.

Gold-based compounds have emerged as a promising class of anticancer agents as an alternative to Pt-based drugs.[15–18] However, the clinical use of these potential drugs has been until now hampered by a series of factors, including their low solubility and stability in aqueous media.[15–18] Greater solubility and stability could be obtained by encapsulation of gold-based drugs within a protein nanocage. Ft-gold drug adducts could also have the advantage of enhanced selectivity for tumor cells.[19]

Recently, we have successfully encapsulated the gold-based drug $[Au_2(bipy^{Me})_2(\mu\text{-}O)_2][PF_6]_2$ ($bipy^{Me}$ = 6-methyl-2,2′-bipyridine), **Auoxo3**, with a AFt nanocage.[19] The drug-loaded protein is cytotoxic towards different malignant cells (HeLa, MCF-7 and HepG2) and shows a lower toxicity for non-malignant cells (H9c2, HRCE and HaCaT).[19] The incorporation of **Auoxo3** inside the cage leads to the formation of gold(I) ions that bind AFt close to the side chains of Cys126, Cys48, His49, His132, and His147. The UV-Vis spectrum of **Auoxo3**-encapsulated AFt also suggests the formation of a small amount of gold nano-

[a]*Department of Chemical Sciences, University of Naples Federico II, Complesso Universitario di Monte Sant'Angelo, Via Cintia, I-80126, Napoli, Italy. E-mail: antonello.merlino@unina.it; Fax: +39 081674090; Tel: +39 081674276*
[b]*Department of Chemistry and Pharmacy, University of Sassari, Italy*
†Electronic supplementary information (ESI) available. See DOI: 10.1039/c7dt02370g

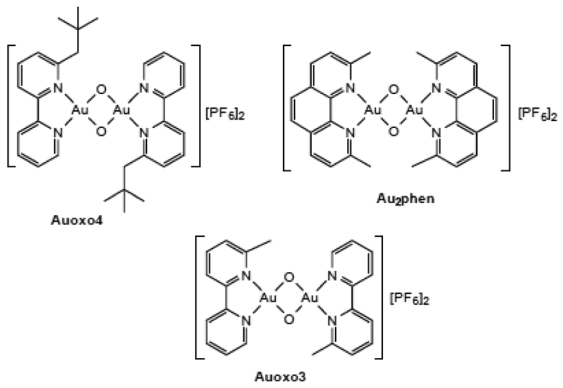

Fig. 1 Structure of selected gold(III) compounds of interest for their antitumor action.

particles (Fig. S3 in the ESI of ref. 19), which absorb at 548 nm, in agreement with what has recently been observed for gold nanoparticles formed upon the reduction of a $AuCl_4^-$ encapsulated Ft variant with $NaBH_4$.[20]

Here, we have encapsulated two other gold-based drugs of medicinal interest, namely $[Au_2(bipy^{nP})_2(\mu\text{-}O)_2][PF_6]_2$ ($bipy^{nP}$ = 6-*neo*-pentyl-2,2′-bipyridine), **Auoxo4**, and $[Au_2(Me_2phen)_2(\mu\text{-}O)_2][PF_6]_2$ (Me_2phen = 2,9-dimethyl-1,10-phenanthroline), **Au_2phen**, (Fig. 1) in an AFt nanocage. **Auoxo4** and **Au_2phen** are both more cytotoxic than **Auoxo3**,[17,21–24] and thus we expect an increased cytotoxicity of these Ft adducts when compared to the previously characterized **Auoxo3**-encapsulated AFt. X-ray structures of **Au_2phen**- and **Auoxo4**-encapsulated AFts were solved and the cytotoxicity of the two adducts was assessed by MTT assay on human MCF-7 and HeLa cancer cell lines and on non-cancer cells H9c2 and HaCaT. The data indicate that gold nanoparticles are not formed inside **Au_2phen**- and **Auoxo4**-encapsulated AFt cages. New adducts are much more cytotoxic than the **Auoxo3**-encapsulated AFt. The activation of oxidative stress and of apoptosis in MCF-7 cells treated with **Au_2phen**-loaded AFt is also reported.

Results

Preparation and characterization of gold compound-encapsulated AFt

The potential antitumor drug-loaded nanostructure was prepared using the procedure previously described by Huang *et al.*[14] and already used to encapsulate cisplatin,[9] carboplatin[10] and the gold-based drug **Auoxo3**,[19] which belongs to the **Auoxos**, *i.e.* a series of dinuclear gold(III) oxo-bridged complexes supported by substituted 2,2′-bipyridine (*e.g.* 6-methyl-2,2′-bipyridine and 6-*neo*-pentyl-2,2′-bipyridine in **Auoxo3** and **Auoxo4**, respectively) or 1,10-phenanthroline (*e.g.* 2,9-dimethyl-1,10-phenanthroline in **Au_2phen**) ligands.[20–22,23,24]

The Ft cage can be disassembled at both acidic and basic pH values. We have preferred the protocol using the basic pH, so that we can directly compare our new data with those previously obtained with **Auoxo3**.[19]

Thus, in order to disassemble the Ft cage into subunits, horse spleen ferritin was incubated for 20 minutes at pH 13 after adding NaOH up to a final concentration of 0.1 M. This solution was then mixed with powdered **Au_2phen** and **Auoxo4** and the two samples were incubated for 30 minutes at room temperature under stirring. Then, pH was decreased to 7.4 using 1.0 M sodium phosphate. The two gold-encapsulated samples were then dialysed through ultracentrifugation on centricon filters (10 kDa cutoff) to remove the excess drugs. To confirm the encapsulation of gold compounds within the Ft shell and verify that upon encapsulation the protein re-assembles readopting its native conformation, UV-Vis absorption spectroscopy (Fig. 2A), circular dichroism (Fig. 2B) and inductively coupled plasma mass spectrometry (ICP-MS) data were collected.

UV-Vis spectra of **Au_2phen** and **Auoxo4**-encapsulated AFt were compared with those of AFt, used as a control, and of **Auoxo3**-encapsulated AFt. Contrary to what was found for

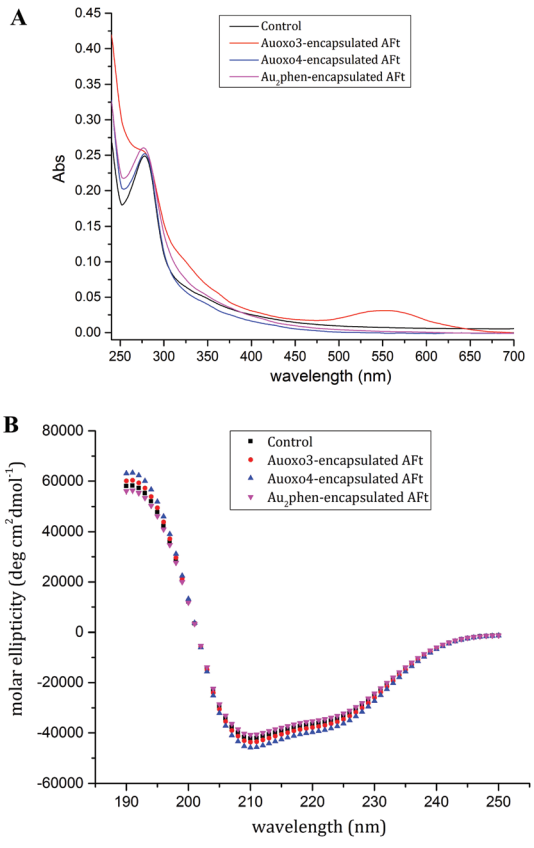

Fig. 2 UV-Vis absorption spectra (A) and far-UV CD spectra (B) of gold-encapsulated Fts compared to the drug-free protein (control). UV-Vis spectra were acquired using a protein concentration of 0.25 mg mL^{-1} in 10 mM sodium phosphate at pH 7.4. Far-UV CD spectra were acquired using a protein concentration of 0.1 mg mL^{-1} in 10 mM sodium phosphate at pH 7.4. The superposition of the curves in the region between 250 nm and 280 nm confirms that the drugs are successfully encapsulated in the nanocage.

Auoxo3-encapsulated AFt (see Fig. 2A),[19] there is no absorption at 548 nm in the UV-Vis spectra of the new encapsulated AFts, indicating that gold nanoparticles are not formed when these two compounds are within AFt. This indication was further supported by the inspection of the colour of the **Auoxo4**- and **Au$_2$phen**-encapsulated AFt solutions, which appear light yellow and remain in this colour for weeks, at variance with that of **Auoxo3**-encapsulated AFt which turns violet with time (Fig. S1†). The ICP-MS data indicate that the Ft nanocage can encapsulate 0.6 to 24 gold atoms per subunit, depending on the preparation. The data reported in this paper were collected for the samples of **Auoxo4**- and **Au$_2$phen**-encapsulated AFt solutions containing 16 and 18 atoms of gold per Ft chain, *i.e.* 384 and 432 Au atoms per cage in the case of **Auoxo4** and **Au$_2$phen**, respectively. Interestingly aged-samples of **Au$_2$phen**-encapsulated AFt (10 months) retain the same amount of gold inside the cage when compared to freshly prepared samples.

Far-UV circular dichroism measurements reveal that the initial Ft secondary structure content was restored upon the encapsulation procedure (Fig. 2B).

X-ray structure analysis of Auoxo4-encapsulated AFt and Au$_2$phen-encapsulated AFt

As indicated by Tosi and co-workers,[25] the effective clinical translation of drug-encapsulated Ft nanocages is probably limited also by the poor knowledge of the consequence of the protocols used to encapsulate the drugs on the overall architecture and structure of the nanocage. Circular dichroism is the technique that was most frequently used to evaluate the effects of the encapsulation protocols on the Ft structure. Although this technique provides reliable information on the secondary structure content of Ft, it does not show a real representation of the integrity of the cage after the disassembly/assembly process. X-ray crystallography is certainly the best choice to characterize the structure of the adducts. The X-ray structures of **Au$_2$phen**-encapsulated AFt and **Auoxo4**-encapsulated AFt were solved at 1.82 and 2.60 Å resolution, respectively (Fig. 3A) and compared with those of a ligand-free protein and of the adduct formed upon the encapsulation of **Auoxo3**. The two structures were solved using the structure of the drug-free protein as a starting model and refined to an R_{factor} of 0.161 and 0.184 and an R_{free} of 0.187 and 0.236, respectively.

Positions of gold atoms in the structure were unambiguously identified by inspection of anomalous and 2Fo-Fc e.d. maps.

The structures are very similar to each other: they superimpose with a root mean square deviation between carbon alpha atoms of 0.38 Å. The structures of both **Au$_2$phen**-encapsulated AFt and **Auoxo4**-encapsulated AFt present two gold atoms bound to the side chains of Cys126 (Fig. 3B), whereas that of **Auoxo3**-encapsulated AFt shows gold atoms bound to the side chains of Cys126, Cys48, His49, His132, and His147.[19]

The geometry around the metal centres is linear, indicating that gold is probably in the oxidation state +1. The extensive degradation of the compounds and the reduction of the gold atom from +3 to +1 are not surprising since they were already

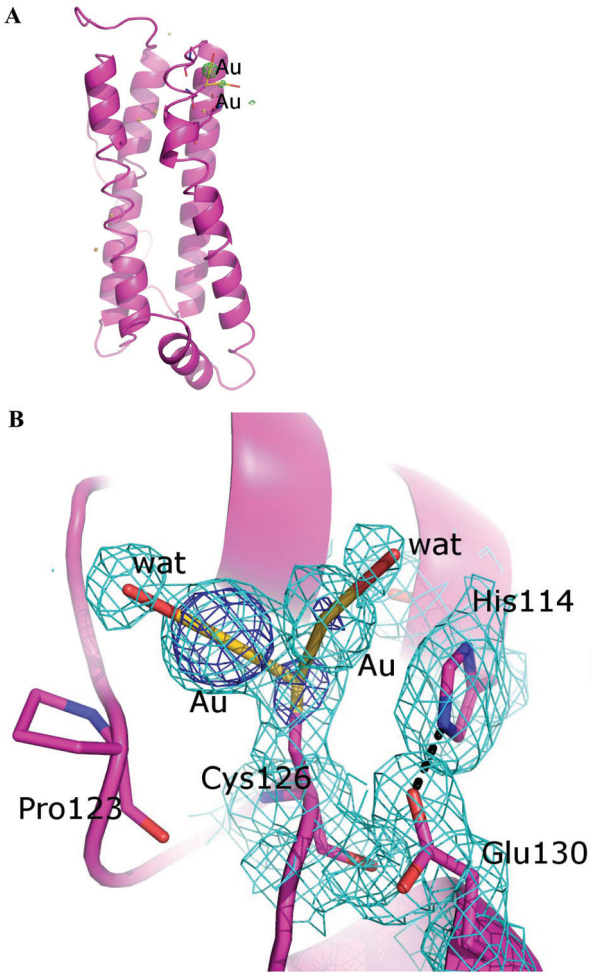

Fig. 3 Overall structure of the **Au$_2$phen**-encapsulated AFt subunit with the Bijvoet difference Fourier map calculated with the anomalous data and reported at 4σ (A). An enlargement of the gold binding site region with the anomalous map is reported in Fig. S2.† In panel B, 2Fo-Fc electron density maps at 0.8σ (cyan) and 4σ (blue) of gold ions coordinated to Cys126 are reported. The gold ions were refined with partial occupancy (0.50 and 0.30); the average *B*-factors for gold ions are in the range 16.7–48.1 Å^2. Similar results were obtained for **Auoxo4**-encapsulated AFt (Fig. S3 and S4†). The structures were deposited in the Protein Data Bank under accession codes 6ENW and 6ENV.

observed in many other adducts of gold(III) based drugs with proteins, including members of the **Auoxo** series.[26–29]

We have searched for the origin of the different behaviour of **Auoxo3**, when compared to **Auoxo4** and **Au$_2$phen**, in the biophysical properties of the three compounds. **Auoxo3** and **Auoxo4** are structurally very similar and have similar redox potentials (**Auoxo3**: E_p = −0.41 V *vs.* SCE in DMSO, corresponding to E_p = −0.39 V *vs.* NHE in aqueous solutions; **Auoxo4**: E_p = −0.40 V *vs.* SCE in DMSO, corresponding to E_p = −0.38 V *vs.* NHE in aqueous solutions). However, these two structurally related compounds show a different rate of hydrolysis reaction, which probably precedes the reduction process (half-life time at 70 °C ($t_{1/2}$) = about 1 h and 9 h for **Auoxo3** and **Auoxo4**, respectively). This difference, which we believe

could be the basis of the different behaviour of the two compounds, should be attributed to the presence of a large, hydrophobic, neopentyl group in the structure of **Auoxo4**, which protects the Au atom from the nucleophilic attack by water molecules (or by OH^- at alkaline pH) more effectively than the small methyl group.

Au_2phen behaves differently when compared to **Auoxo3** probably because of its highly negative redox potential (E_{pc1} = −0.946 V and E_{pc2} = −1.329 V *vs.* F_c^+/F_c at a scan rate of 0.1 V s^{-1}),[23] which indicates high redox stability. Thus, both **Au_2phen** and **Auoxo4** have a lower tendency for reduction than **Auoxo3** and this could explain both the lower number of gold(I) binding sites observed in the structure of the encapsulated AFts here reported when compared to **Auoxo3**-encapsulated AFt and the higher tendency of **Auoxo3** to form gold nanoparticles inside the Ft cage when compared to **Au_2phen** and **Auoxo4**.

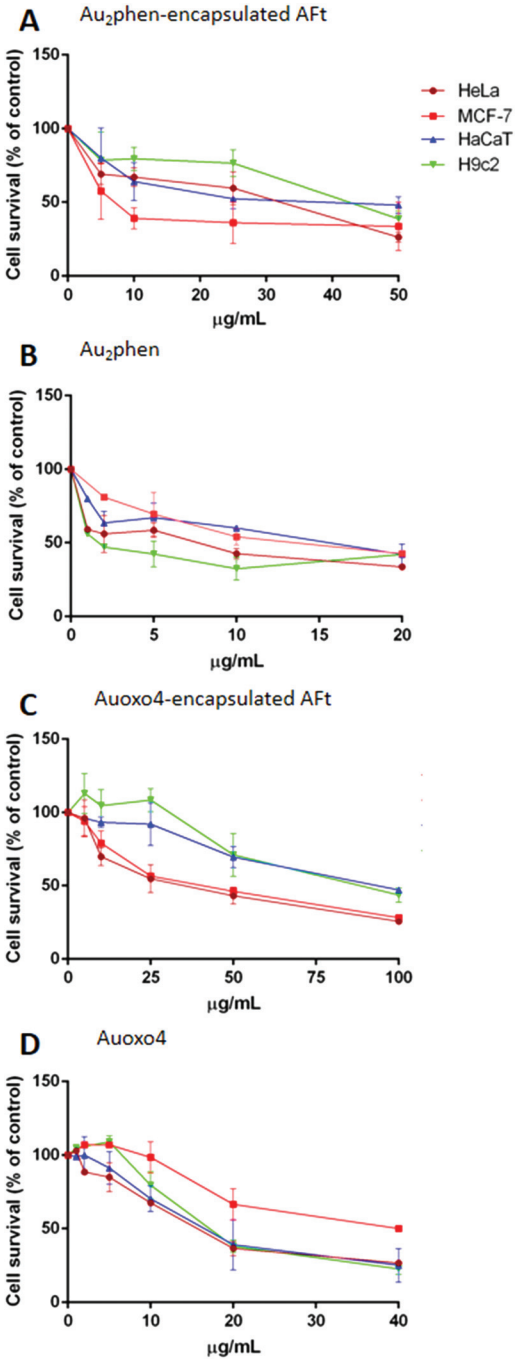

Fig. 4 Effects of **Au_2phen**-encapsulated AFt (A), **Au_2phen** (B), **Auoxo4**-encapsulated AFt (C) and **Auoxo4** (D) on human cancer (HeLa and MCF-7) and normal cells (HaCaT and H9c2). The cells were treated with increasing amounts of the cage and of the free drug for 48 hours. Cell viability was assessed by the MTT assay and expressed as described in the Materials and methods section. All values are given as means ± SD.

Cytotoxicity

To assess the cytotoxic effect of **Auoxo4**- and **Au_2phen**-encapsulated AFts to inhibit cell growth, different cell lines were analysed. In particular, two cancer cell lines, human epithelial breast (MCF-7) and cervix carcinoma (HeLa) cells, and two normal cell lines, rat cardiomyoblasts (H9c2) and human keratinocytes (HaCaT) were used. The cells were incubated for 48 h with increasing concentrations of **Auoxo4**- and **Au_2phen**-encapsulated AFts, as well as with increasing concentrations of the free gold-based drugs. Then the ability of functional mitochondria to catalyse the reduction of MTT to form formazan salt by mitochondrial dehydrogenases was evaluated.[30] Drug-free Ft has already been used as a control in a previous paper and it did not show significant toxicity to any of the analysed cell lines.[19]

The results obtained after 48 h of incubation of cells with the new adducts are reported in Fig. 4 and show typical dose–response curves. The corresponding IC_{50} values, summarized in Table 1, indicate that, after 48 h incubation, encapsulated nanocages are more toxic towards cancer cell lines than towards normal cells. It is particularly interesting to underline that the presence of the cage significantly reduces the toxicity of the free gold drugs towards the non-cancer cell lines, enhancing the selectivity of the gold compounds towards tumour cells. Moreover, the new encapsulated AFts are more active than the **Auoxo3**-encapsulated AFt, for which IC_{50} values were determined after 72 h.[19]

In this respect, it is noteworthy that there are differences in the cytotoxicity profiles of the two gold-encapsulated AFts that are probably due to the different amounts of gold that is

Table 1 IC_{50} values (μM) obtained for **Au_2phen**, **Auoxo4** and **Au_2phen**- and **Auoxo4**-encapsulated AFts in HeLa, MCF-7, H9c2 and HaCaT cell lines. Concentrations refer to the amount of gold

IC_{50}, μM, 48 h	**Au_2phen**-encapsulated AFt	**Au_2phen**	**Auoxo4**-encapsulated AFt	**Auoxo4**
HeLa	32 ± 4	6.5 ± 1.0	23 ± 9	13.74 ± 0.96
MCF-7	6 ± 1	10.6 ± 2.5	30 ± 1	34.8 ± 4.3
H9c2	40 ± 1	1.28 ± 0.06	68 ± 6	14.6 ± 1.4
HaCaT	36 ± 9	14.3 ± 1.7	73 ± 6	12.4 ± 1.6

encapsulated within the Ft and thus internalized by the cells. Moreover, it should also be recalled that since the structures of **Auoxo4**- and **Au$_2$phen**-encapsulated AFts are similar, the differences should be due to the gold compounds that are within the cage, *i.e.* in the bulk. Interestingly, cytotoxicity experiments carried out on an aged-sample of **Au$_2$phen**-encapsulated AFt (10 months) lead to results that are very similar to those obtained by using freshly prepared samples, thus suggesting a high stability of the protein adduct.

Uptake data

To obtain a deeper insight into the amount of gold that is internalized by the cells, ICP-MS data on the uptake of **Au$_2$phen** and **Au$_2$phen**-encapsulated AFt, tested at the concentration needed to reach IC_{50} values, were collected. We found that the amount of gold uptake by MCF-7 cells is variable with **Au$_2$phen**, with values ranging from 2.2 μg up to 12.8 μg of gold per 1.5×10^6 cells, whereas it is constant in the case of **Au$_2$phen**-encapsulated AFt, with values close to 0.06 μg of gold per 1.5×10^6 cells. These data indicate that the use of Ft strongly reduces the gold uptake and that the amount of Au internalized by the cells needed to kill 50% of them when they are treated with the free drug is 30–100 times higher than that needed when the cells are treated with **Au$_2$phen**-encapsulated AFt. Moreover, it is found that the **Au$_2$phen**-encapsulated AFt is slightly more cytotoxic than the free gold complex. These findings indicate that the mode of action of the drug encapsulated within the cage is significantly different and more efficient when compared to that of the free drug, which enters the cells *via* passive diffusion. Further studies are needed to deeply analyse the reason for the greater cytotoxicity of **Au$_2$phen**-encapsulated AFt when compared to the free gold complex and the exact mechanism of action of these potential gold-based drugs.

Au$_2$phen-encapsulated AFt induces oxidative stress and apoptosis in MCF-7 human breast cancer cells

As it has been recently reported that ferrocenylated N-heterocyclic carbene supported gold(I) compounds are able to induce oxidative stress and subsequent cell death in cancer lung cells,[31] we analysed if **Au$_2$phen**-encapsulated AFt, which is endowed with the highest cytotoxic activity toward malignant cells, was able to alter the redox state of MCF-7 (the most sensitive cells to **Au$_2$phen**-encapsulated AFt). As shown in Fig. 5A, we found an increase in ROS levels after 6 h of incubation with **Au$_2$phen**-encapsulated AFt and the drug alone, whereas no effect was observed for drug-free AFt. It is known that mitochondria are sensitive to changes in the cellular redox status and ROS activation is known to induce depolarization of the mitochondrial membrane.[32] For this reason, we measured the mitochondrial potential of MCF-7 cells after **Au$_2$phen**-encapsulated AFt and **Au$_2$phen** treatment by TMRE (Mitochondrial Membrane Potential) assay[33] overtime (Fig. 5B).

We observed that after 6 h of incubation, the fluorescence intensity significantly decreases in the cells treated with

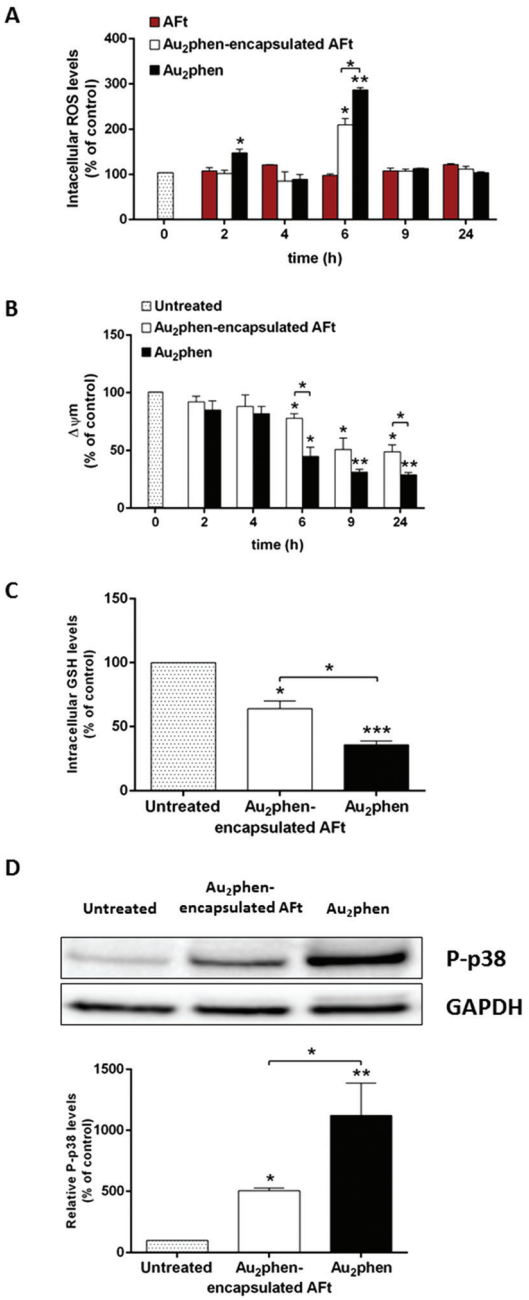

Fig. 5 Activation of the oxidative stress pathway in MCF-7 cells after treatment with **Au$_2$phen**-encapsulated AFt and **Au$_2$phen**. MCF-7 were incubated in the presence of 7 μg mL^{-1} of **Au$_2$phen**-encapsulated AFt and 12 μg mL^{-1} of **Au$_2$phen** for different lengths of time (2 to 24 h) and markers of the oxidative stress were evaluated. Time-dependent changes in ROS levels were detected with a DCFDA probe and expressed as the fluorescence intensity percentage over control (%) (panel A). Time-dependent changes in the mitochondrial membrane potential ($\Delta\psi_m$) were determined using TMRE staining and expressed as the TMRE fluorescence intensity over control (%) (panel B). Intracellular GSH levels were determined by DTNB assay after 6 h of incubation. Values are expressed as a fold increase with respect to control cells (panel C). Western blotting of the phosphorylation level of p38 (upper panel) after 24 h of incubation, with the relative densitometric analysis (panel D). GAPDH (lower panel) was used as an internal standard. The data shown are the means ± S.D. of three independent experiments. * indicates $p < 0.001$, ** indicates $p < 0.0001$, *** indicates $p < 0.00001$.

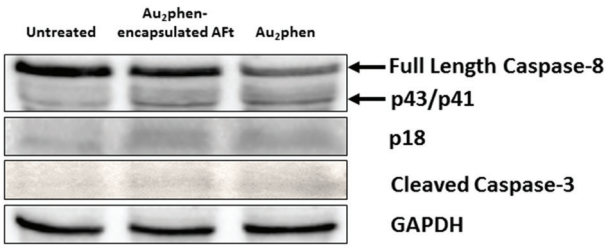

Fig. 6 Apoptosis activation in MCF-7 incubated with **Au_2phen**-encapsulated AFt and **Au_2phen**. The cells were incubated for 48 h in the presence of 7 μg mL^{-1} of **Au_2phen**-encapsulated AFt and 12 μg mL^{-1} of **Au_2phen** and then cell extracts were prepared and subjected to western blotting analysis. Western blotting was performed using anti Caspase-3, which recognizes the activated form of the protein and anti Caspase-8, which recognizes pro-Caspase-8 and the activated forms (p43/41 and p18). GAPDH was used as the loading control.

Au_2phen and **Au_2phen**-encapsulated AFt, when compared to untreated cells, thus suggesting that the treatment results in the dissipation of the mitochondrial membrane potential ($\Delta\psi m$). However, the lowest permeability threshold was found after 9 h of treatment and remained constant up to 24 h of incubation. This implies mitochondrial damage during treatment with the **Au_2phen**-encapsulated AFt and drug alone.

Furthermore, a decrease in intracellular GSH levels after 6 h of treatment (Fig. 5C) and the increase in the phosphorylation level of p38, a protein involved in inflammation, cell cycle, development, differentiation and death, senescence and tumorgenesis[34] confirmed the activation of the oxidative stress pathway (Fig. 5D).

We finally analysed if apoptosis occurred in our experimental system, since it is known that cells are driven to apoptosis when ROS levels become too high.[31,35] The cells were incubated for 48 h in the presence of **Au_2phen**-encapsulated AFt and **Au_2phen** and the activation of Caspases 8 and 3 was analysed. As shown in Fig. 6, both Caspases were activated after 48 h incubation.

We hypothesize that apoptosis is triggered by the release of the drug inside the cell, in agreement with the data obtained by Zhang *et al.* who have demonstrated that Ft can be internalized through TfR1 and can dissociate and release its cargo upon acidification of the endosomal compartment.[36]

Materials and methods

Sample preparation

Horse spleen ferritin was purchased from Sigma (code F4503, about 90% L chain) and used without further purification. A stock solution of Ft was stored at 4 °C in 0.15 mM sodium chloride. Gold based drugs **Auoxo4** and **Au_2phen** were synthesized as previously described.[20–22,23] **Au_2phen**-encapsulated AFt and **Auoxo4**-encapsulated AFt were prepared using the same procedure, *i.e.* following the protocol we have already used to encapsulate cisplatin,[9] carboplatin[10] and gold-based drug **Auoxo3**.[19] The AFt protein nanocage was first dissociated into individual subunits at pH 13, using NaOH (final concentration 0.1 M), in the presence of the drug (protein to gold compound molar ratio 1 : 50), and then reassembled at pH 7.4 using 1.0 M sodium phosphate buffer. During the reassembly process, gold compounds were trapped within the inner cavity of the cage. The reaction solution was slowly stirred during all steps. The final solution was ultracentrifuged at 5000 rpm to remove the abundant precipitate and the supernatant recovered was then dialyzed using centricon filters (10 kDa cutoff) against 10 mM sodium phosphate buffer, pH 7.4 to remove the excess of the drug that is unbound.

Analytical and biophysical characterization of the samples

ICP-MS data were collected to confirm the encapsulation of gold compounds inside the cages, to quantitatively evaluate the efficiency of the gold compound encapsulation and estimate the amount of gold inside the cells. Gold standard solutions were prepared in 5% HNO_3 at 4 different concentrations (1, 10, 50, and 100 μg L^{-1}). The Au concentration was measured. All the analyses were performed in triplicate.

To determine the amount of gold inside the cells, treated and untreated cells were extensively washed with PBS and aliquots of the medium of treated and untreated cells and their cell pellets were incubated with 200 μl of 65% HNO_3 (Sigma Aldrich) and 600 μl of 35% HCl (Sigma Aldrich) overnight at 90 °C. The solution was then transferred into polystyrene liners, diluted at 1 : 10 v/v with 5% HNO_3 and finally analysed with an Agilent 7700 ICP-MS from Agilent Technologies, equipped with a frequency-matching RF generator and a 3rd generation Octopole Reaction System (ORS3), operating with helium gas in ORF. The following parameters were used: radio-frequency power 1550 W, plasma gas flow 14 L min^{-1}; carrier gas flow 0.99 L min^{-1}; He gas flow 4.3 mL min^{-1}. ^{103}Rh was used as an internal standard (final concentration: 50 μg L^{-1}). The error in the determination of the amount of gold within the cells is within 10%.

The data indicate that **Auoxo4**-encapsulated AFt and **Au_2phen**-encapsulated AFt contained a variable Ft subunit to Au ratio, depending on the preparation, and an undetectable amount of iron, confirming that the protein is in the Apo form (AFt) in the final adduct.

The gold compound-encapsulated AFts were also characterized by obtaining UV-Vis absorption and circular dichroism spectra.

UV-Vis absorption spectra were recorded on a Jasco V650 UV-visible spectrophotometer in 10 mM sodium phosphate at pH 7.4 by using the protein at a concentration of 0.25 mg mL^{-1}. Experimental conditions: 240–700 nm wavelength range, 200 nm min^{-1} scanning speed and 1 nm data pitch.

CD spectra were recorded on a Jasco V815 spectropolarimeter in the 190–250 nm range using a protein concentration of 0.1 mg mL^{-1} in 10 mM sodium phosphate at pH 7.4. Experimental conditions: 2 nm bandwidth, 50 nm min^{-1} scanning speed, 1 nm data pitch and 4 s response time.

Crystallization and X-ray diffraction data collection

Auoxo4- and **Au_2phen**-encapsulated AFts were crystallized by the hanging-drop vapor diffusion method at 298 K: 1 μL drops of 5 to 10 mg mL^{-1} protein adduct were mixed with equal volumes of 0.6–0.8 M $(NH_4)_2SO_4$, 0.1 M Tris HCl pH 7.4–7.7, and 50–60 mM $CdSO_4$.

X-ray diffraction data were collected from single crystals at 100 K at CNR Institute of Biostructure and Bioimages, Naples, Italy, as previously done for **Auoxo3**-encapsulated AFt.[19] Datasets were processed with HKL2000.[37] The results are summarized in Table S1.†

Structure resolution and refinement

Phases have been obtained by molecular replacement using the program Phaser[38] and the coordinates of the protein extracted from the PDB file 5ERK[9] as a starting model. The refinement of atomic positions and individual *B*-factor were carried out using Refmac5.7.[39] The inspection of the structure and analysis of the electron density maps were performed using Wincoot.[40] Gold atoms were identified as previously described, *i.e.* considering anomalous, 2Fo-Fc and Fo-Fc electron density maps. Details of the assignment of Au *versus* Cd ions are reported in Table S2.† The structures' final models are refined at 1.82 and 2.60 Å resolution to a R_{factor} of 0.161 and 0.184 and a R_{free} of 0.187 and 0.236, respectively. Refinement statistics are reported in Table S1.† Coordinates and structure factors were provided to reviewers and the editor for the review process and deposited in the Protein Data Bank under the accession codes 6ENW and 6ENV, respectively. Uninterpreted peaks of electron density in the Fo-Fc electron density maps are discussed in Table S3.†

Cell culture and MTT assay

Human breast cancer cells (MCF-7), cervical cancer cells (HeLa) and rat cardiomyoblast cells (H9c2) were obtained from ATCC. Human keratinocyte cells (HaCaT) were obtained from Innoprot. All cell lines were cultured in Dulbecco's Modified Eagle's Medium (Sigma-Aldrich, St Louis, Mo, USA), supplemented with 10% foetal bovine serum (HyClone), 2 mM L-glutamine and antibiotics, all from Sigma-Aldrich, under a 5% CO_2 humidified atmosphere at 37 °C. The growth medium of H9c2 cells was implemented with 2 mM L-glutamine and 2 mM sodium pyruvate. For dose–response and time-course experiments, cells were seeded in 96-well plates at a density of 2×10^3 cells per well. 24 h after seeding, increasing concentrations of compounds were added to the cells. Cell viability was assessed by the MTT (3-(4,5-dimethylthiazol-2-yl)-2,5-diphenyltetrazolium bromide) assay, as described by Monti *et al.*[41] Cell survival was expressed as the percentage of viable cells in the presence of the drug compared to controls. Two groups of cells were used as controls, *i.e.* cells untreated with the drug and cells supplemented with identical volumes of buffer. Each sample was tested in three independent analyses, each carried out in triplicate.

Oxidative stress analyses

To estimate ROS production, the protocol described by Petruk[42] was followed, with some modifications. Briefly, MCF-7 cells were incubated with 7 μg mL^{-1} of **Au_2phen**-encapsulated AFt and 12 μg mL^{-1} of **Au_2phen** alone, for different lengths of time (0–24 h) and then incubated with 2′,7′-dichlorodihydrofluorescein diacetate (H_2-DCFDA, Sigma-Aldrich). Fluorescence intensity was measured by using a PerkinElmer LS50 spectrofluorometer (525 nm emission wavelength, 488 nm excitation wavelength, 300 nm min^{-1} scanning speed and 5 nm slit width for both excitation and emission). ROS production was expressed as a percentage of DCF fluorescence intensity of the sample under test, with respect to the untreated sample. Each value was assessed by three independent experiments, each with three determinations. Significance was determined by Student's *t*-test.

To analyse the mitochondrial membrane potential ($\Delta\psi_m$) the cells were plated at a density of 2×10^4 cells per well and after 24 h were treated as described above. At the end of treatment, the cells were incubated with 200 nM cationic lipophilic dye tetramethylrhodamine ethyl ester (TMRE) for 20 min at 37 °C. Then, the cells were gently washed with 0.2% BSA in PBS three times and the fluorescence was measured in a microplate reader with peak E_x/E_m = 549/575 nm. Each value is the mean of three independent experiments, each with three determinations. Significance was determined by Student's *t*-test.

To estimate intracellular glutathione levels, the cells were plated and treated as described above and then incubated at 37 °C for 6 h. At the end of the incubation, DTNB assay was performed as described by Petruk *et al.*[42] Briefly, the cells were detached with trypsin and lysed and the protein concentration was determined by the Bradford assay. Then, 50 μg of proteins were incubated with 3 mM EDTA and 144 μM 5,5′-dithiobis-2-nitrobenzoic acid (DTNB) in 30 mM Tris-HCl pH 8.2 and centrifuged and the absorbance of the supernatant was measured at 412 nm by using a multiplate reader (Biorad). GSH levels were expressed as the percentage of TNB absorbance in the sample under test with respect to the untreated sample. Values are the mean of three independent experiments, each with triplicate determination. Significance was determined by Student's *t*-test.

For western blotting analyses, the cells were plated at a density of 2×10^4 cells per cm^2 in complete medium for 24 h and then treated as described above. After 48 h of incubation, cell lysates were analysed by western blotting performed as reported by Galano *et al.*[43] Antibodies for phospho-p38, activated CASP-3 and CASP-8 were purchased from Cell Signal Technology (Danvers, MA, USA). To normalize protein intensity levels, a specific antibody against internal standards was used, *i.e.* anti-GAPDH (Thermo Fisher, Rockford, IL, USA). The chemiluminescence detection system (SuperSignal® West Pico) was from Thermo Fisher.

Conclusions

Ferritin has been used as a scaffold for the fabrication of gold nanoparticles and for the encapsulation of a variety of mole-

cules, including metallodrugs. Here, taking advantage of the reversible dissociation of Ft at alkaline pH, we have encapsulated two different gold-based anticancer compounds (**Au_2phen** and **Auoxo4**), belonging to the **Auoxos** series, within the ferritin nanocage and have characterized the adducts formed by X-ray crystallography. The cytotoxicity of these adducts has been evaluated on different cell lines. The data have been compared with those obtained for **Auoxo3**-encapsulated AFt. As expected, **Auoxo4**- and **Au_2phen**-encapsulated AFts exhibit higher cytotoxicity than **Auoxo3**-encapsulated AFt, showing high cytotoxicity to MCF-7 and HeLa cell lines in a dose-dependent manner. The adducts show moderate selectivity, since they kill tumour cell lines at a lower concentration than that needed to kill normal cell lines. The structures of the two adducts do not reveal significant differences, indicating that the differences in the cytotoxicity of the gold-encapsulated AFt depend mainly on the intrinsic properties of the encapsulated compounds rather than on the structure of the ferritin adduct obtained upon encapsulation. In contrast, both the structural and biological features of the new encapsulated AFts are different when compared to those previously reported for **Auoxo3**-encapsulated AFt. Differences are attributed to the diverse propensity of these gold drugs to undergo hydrolysis and successive reduction.

Surprisingly, the uptake data indicate that the amount of gold internalized by MCF-7 cells is higher when the cells are treated with the free drug than in the case of **Au_2phen**-encapsulated AFt. This suggests that internalization of **Au_2phen**-encapsulated AFt into cancer cells, which probably occurs *via* receptor-mediated endocytosis, is less efficient when compared to the passive diffusion of the free drug. However, the drug-loaded AFt nanocages are more selective than free drugs in killing cancer cells; the selectivity may reside in the different mechanisms of endocytosis of the two molecules. At present, the origin of the specificity of the ferritin nanocages and of its higher cytotoxicity when compared to the free drug is still unknown and will be the subject of further investigations. It is also unknown if horse spleen apoferritin (composed of 85% L chains and 15% H chains) enters the cell *via* TfR1 and/or Scara5 receptors. Geninatti Crich *et al.* reported that the chimeric nanocage enters the cell *via* Scara5,[44] whereas Zhang and co-workers reported that the internalization of the H/L-chimeric Ft nanocage was due to TfR1.[36] The higher expression of both receptors on the cancer cell surface, with respect to normal cells, could give specificity to the treatment, as supported by the different IC_{50} values obtained for cancer and normal cells.

Finally, we have demonstrated that **Au_2phen**-encapsulated AFt is able to alter MCF-7 cell redox homeostasis, thus inducing apoptosis activation. We hypothesize that the lower sensitivity of normal cells to **Au_2phen**-encapsulated AFt can be due to the higher ability of adaptation of normal cells to counteract the negative effects of oxidative stress and, in turn, to cell death.

Conflicts of interest

There are no conflicts to declare.

Acknowledgements

The authors thank G. Sorrentino and M. Amendola for technical assistance at CNR Institute of Biostructures and Biomages and N. Pontillo for his help in the preliminary characterization of the encapsulated AFts. MAC kindly acknowledges Regione Autonoma della Sardegna (RAS) for the financial support from L. R. 7, CRP-78365; A. M. acknowledges the University of Naples Federico II for financial support (000005-ALTRI_DR_409_2017_Rec_Ateneo).

References

1 M. Uchida, S. Kang, C. Reichhardt, K. Harlen and T. Douglas, *Biochim. Biophys. Acta, Gen. Subj.*, 2010, **1800**, 834–845.
2 S. C. Andrews, P. Arosio, W. Bottke, J. F. Briat, M. Vondarl, P. M. Harrison, J. P. Laulhere, S. Levi, S. Lobreaux and S. J. Yewdall, *J. Inorg. Biochem.*, 1992, **47**, 161–174.
3 M. Uchida, M. L. Flenniken, M. Allen, D. A. Willits, B. E. Crowley, S. Brumfield, A. F. Willis, L. Jackiw, M. Jutila, M. J. Young and T. Douglas, *J. Am. Chem. Soc.*, 2006, **128**, 16626–16633.
4 J. Xie, Z. P. Zhen and W. Tang, *Cancer Res.*, 2013, **73**(8 Suppl): Abstract nr 4513, DOI: 10.1158/1538-7445.
5 T. Kitagawa, H. Kosuge, M. Uchida, M. M. Dua, Y. Iida, R. L. Dalman, T. Douglas and M. V. McConnell, *Mol. Imaging Biol.*, 2012, **14**, 315–324.
6 D. Hogemann-Savellano, E. Bos, C. Blondet, F. Sato, T. Abe, L. Josephson, R. Weissleder, J. Gaudet, D. Sgroi, P. J. Peters and J. P. Basilion, *Neoplasia*, 2003, **5**, 495–506.
7 L. Mendes-Jorge, D. Ramos, A. Valenca, M. Lopez-Luppo, V. M. R. Pires, J. Catita, V. Nacher, M. Navarro, A. Carretero, A. Rodriguez-Baeza and J. Ruberte, *PLoS One*, 2014, **9**, e106974.
8 J. Y. Li, N. Paragas, R. M. Ned, A. D. Qiu, M. Viltard, T. Leete, I. R. Drexler, X. Chen, S. Sanna-Cherchi, F. Mohammed, D. Williams, C. S. Lin, K. M. Schmidt-Ott, N. C. Andrews and J. Barasch, *Dev. Cell*, 2009, **16**, 35–46.
9 N. Pontillo, F. Pane, L. Messori, A. Amoresano and A. Merlino, *Chem. Commun.*, 2016, **52**, 4136–4139.
10 N. Pontillo, G. Ferraro, H. H. R. Helliwell, A. Amoresano and A. Merlino, *ACS Med. Chem. Lett.*, 2017, **8**, 433–437.
11 Z. P. Zhen, W. Tang, C. L. Guo, H. M. Chen, X. Lin, G. Liu, B. W. Fei, X. Y. Chen, B. Q. Xu and J. Xie, *ACS Nano*, 2013, **7**, 6988–6996.
12 Z. P. Zhen, W. Tang, W. Z. Zhang and J. Xie, *Nanoscale*, 2015, **7**, 10330–10333.
13 Z. P. Zhen, W. Tang, H. M. Chen, X. Lin, T. Todd, G. Wang, T. Cowger, X. Y. Chen and J. Xie, *ACS Nano*, 2013, **7**, 4830–4837.
14 X. T. Ji, L. Huang and H. Q. Huang, *J. Proteomics*, 2012, **75**, 3145–3157.
15 T. Zou, C. T. Lum, C. N. Lok, J. J. Zhang and C. M. Che, *Chem. Soc. Rev.*, 2015, **44**, 8786–8801.

16 C. Nardon, G. Boscutti and D. Fregona, *Anticancer Res.*, 2014, **34**, 487–492.
17 C. Gabbiani, A. Casini and L. Messori, *Gold Bull.*, 2007, **40**, 73–81.
18 B. Bertrand and A. Casini, *Dalton Trans.*, 2014, **43**, 4209–4219.
19 G. Ferraro, D. M. Monti, A. Amoresano, N. Pontillo, G. Petruk, F. Pane, M. A. Cinellu and A. Merlino, *Chem. Commun.*, 2016, **52**, 9518–9521.
20 B. Maity, A. Abe and T. Ueno, *Nat. Commun.*, 2017, **8**, 14820.
21 A. Casini, M. A. Cinellu, G. Minghetti, C. Gabbiani, M. Coronnello, E. Mini and L. Messori, *J. Med. Chem.*, 2006, **49**, 5524–5531.
22 C. Gabbiani, A. Guerri, M. A. Cinellu and L. Messori, *Open Crystallogr. J.*, 2010, **3**, 29–40.
23 M. A. Cinellu, L. Maiore, M. Manassero, A. Casini, M. Arca, H. H. Fiebig, G. Kelter, E. Michelucci, G. Pieraccini, C. Gabbiani and L. Messori, *ACS Med. Chem. Lett.*, 2010, **1**, 336–339.
24 C. Gabbiani, A. Casini, L. Messori, A. Guerri, M. A. Cinellu, G. Mlnghetti, M. Corsini, C. Rosani, P. Zanello and M. Arca, *Inorg. Chem.*, 2008, **47**, 2368–2379.
25 G. Tosi, D. Belletti, F. Pederzoli and B. Ruozi, *Expert Opin. Drug Delivery*, 2016, **13**, 1341–1343.
26 I. Russo Krauss, L. Messori, M. A. Cinellu, D. Marasco, R. Sirignano and A. Merlino, *Dalton Trans.*, 2014, **43**, 17483–17488.
27 L. Messori, F. Scaletti, L. Massai, M. A. Cinellu, I. Russo Krauss, G. di Martino, A. Vergara, L. Paduano and A. Merlino, *Metallomics*, 2014, **6**, 233–236.
28 L. Messori, M. A. Cinellu and A. Merlino, *ACS Med. Chem. Lett.*, 2014, **5**, 1110–1113.
29 L. Messori, F. Scaletti, L. Massai, M. A. Cinellu, C. Gabbiani, A. Vergara and A. Merlino, *Chem. Commun.*, 2013, **49**, 10100–10102.
30 J. C. Stockert, A. Blazquez-Castro, M. Canete, R. W. Horobin and A. Villanueva, *Acta Histochem.*, 2012, **114**, 785–796.
31 J. F. Arambula, R. McCall, K. J. Sidoran, D. Magda, N. A. Mitchell, C. W. Bielawski, V. M. Lynch, J. L. Sessler and K. Arumugam, *Chem. Sci.*, 2016, **7**, 1245–1256.
32 G. Petrosillo, F. M. Ruggiero and G. Paradies, *FASEB J.*, 2003, **17**, 2202–2208.
33 Y. Piao, H. G. Kim, M. S. Oh and Y. K. Pak, *Biochim. Biophys. Acta*, 2012, **1820**, 577–585.
34 D. Munoz-Espin and M. Serrano, *Nat. Rev. Mol. Cell Biol.*, 2014, **15**, 482–496.
35 Y. Zhao, E. B. Butler and M. Tan, *Cell Death Dis.*, 2013, **4**, e532.
36 L. Zhang, L. Li, A. Di Penta, U. Carmona, F. Yang, R. Schops, M. Brandsch, J. L. Zugaza and M. Knez, *Adv. Healthcare Mater.*, 2015, **4**, 1305–1310.
37 Z. Otwinowski and W. Minor, *Methods Enzymol.*, 1997, **276**, 307–326.
38 A. J. McCoy, R. W. Grosse-Kunstleve, P. D. Adams, M. D. Winn, L. C. Storoni and R. J. Read, *J. Appl. Crystallogr.*, 2007, **40**, 658–674.
39 G. N. Murshudov, P. Skubak, A. A. Lebedev, N. S. Pannu, R. A. Steiner, R. A. Nicholls, M. D. Winn, F. Long and A. A. Vagin, *Acta Crystallogr., Sect. D: Biol. Crystallogr.*, 2011, **67**, 355–367.
40 P. Emsley, B. Lohkamp, W. G. Scott and K. Cowtan, *Acta Crystallogr., Sect. D: Biol. Crystallogr.*, 2010, **66**, 486–501.
41 D. M. Monti, D. Guarnieri, G. Napolitano, R. Piccoli, P. Netti, S. Fusco and A. Arciello, *J. Biotechnol.*, 2015, **193**, 3–10.
42 G. Petruk, A. Raiola, R. Del Giudice, A. Barone, L. Frusciante, M. M. Rigano and D. M. Monti, *J. Photochem. Photobiol., B*, 2016, **163**, 284–289.
43 E. Galano, A. Arciello, R. Piccoli, D. M. Monti and A. Amoresano, *Metallomics*, 2014, **6**, 587–597.
44 S. Geninatti Crich, M. Cadenazzi, S. Lanzardo, L. Conti, R. Ruiu, D. Alberti, F. Cavallo, J. C. Cutrin and S. Aime, *Nanoscale*, 2015, **7**, 6527–6533.